Supplement of Atmos. Chem. Phys., 19, 5235–5249, 2019
https://doi.org/10.5194/acp-19-5235-2019-supplement

Atmospheric Chemistry and Physics
Open Access

Supplement of

Characterization of nighttime formation of particulate organic nitrates based on high-resolution aerosol mass spectrometry in an urban atmosphere in China

Kuangyou Yu et al.

Correspondence to: Xiao-Feng Huang (huangxf@pku.edu.cn)

List of supporting information:

Text S1: Nitrate radicals estimation

Figure S1. Time series of PM_1 species for spring (a), summer (b) and autumn (c).

Figure S2. Mass spectrum profiles of 3 factors (a), 4 factors (b) and 5 factors (c) based on PMF analysis, and diagnostic plots of the chosen (3 factors) PMF solution (d) for spring: (1) Q/Qexp vs number of factors; (2) the time series of the measured and the reconstructed organic mass; (3) Q/Qexp vs. FPEAK for the solution with optimal number of factors; (4) the distribution of scaled residuals for each m/z; (5) mass fraction of PMF factors vs. FPEAK; (6) correlations of time series and mass spectra among PMF factors.

Figure S3. Mass spectrum profiles of 3 factors (a), 4 factors (b) and 5 factors (c) based on PMF analysis, and diagnostic plots of the chosen (3 factors) PMF solution (d) for summer: (1) Q/Qexp vs number of factors; (2) the time series of the measured and the reconstructed organic mass; (3) Q/Qexp vs. FPEAK for the solution with optimal number of factors; (4) the distribution of scaled residuals for each m/z; (5) mass fraction of PMF factors vs. FPEAK; (6) correlations of time series and mass spectra among PMF factors.

Figure S4. Mass spectrum profiles of 3 factors (a), 4 factors (b) and 5 factors (c) based on PMF analysis, and diagnostic plots of the chosen (3 factors) PMF solution (d) for autumn: (1) Q/Qexp vs number of factors; (2) the time series of the measured and the reconstructed organic mass; (3) Q/Qexp vs. FPEAK for the solution with optimal number of factors; (4) the distribution of scaled residuals for each m/z; (5) mass fraction of PMF factors vs. FPEAK; (6) correlations of time series and mass spectra among PMF factors.

Figure S5. Diurnal cycles for NR-PM_1 species and OA factors in spring (a), summer (b) and autumn (c)

Figure S6. Mass spectra of the OA factors resolved from the PMF analysis on high-resolution merged organic and nitrate mass spectra (i.e., $PMF_{org+NO3}$ analysis) for (a) spring, (b) summer, (c) autumn and (d) winter.

Figure S7. Scatter plots of $NO_{3.org1\_ratio}$ with HOA and MO-OOA in spring for the whole day (a), at nighttime (b) and during the day (c).

Figure S8. Scatter plots of $NO_{3.org1\_ratio}$ with HOA and MO-OOA in summer for the whole day (a), at nighttime (b) and during the day (c).

Figure S9. Scatter plots of $NO_{3.org1\_ratio}$ with HOA and MO-OOA in autumn for the whole day (a), at nighttime (b) and during the day (c).

Figure S10. Time series of the contributions of CH_2O^+ in m/z 30 and $CH_2O_2^+$ in m/z 46 in the HR data of PM_1 for spring (a), summer (b), autumn (c) and winter (d). (High-resolution mass spectra at m/z 46 only contains NO_2^+ in spring, autumn and winter).

Figure S11. Average size distributions of m/z 30 and m/z 46 in spring (a), summer (b), autumn (c) and winter (d).

Figure S12. Average size distributions of m/z 30/m/z 46 ratio under under highest (>15%) and lowest interferences (<5%) $CH_2O_X^+$ interferences in spring (a), summer (b), autumn (c).

Figure S13. Average size distributions of organic and inorganic nitrates calculated using the size distributions of m/z 30/m/z 46 ratio and NO^+/NO_2^+ ratio method in spring (a), summer (b), autumn (c).

Figure S14. Diurnal trends of relative humidity (RH), temperature, NO_2, O_3 and calculated NO_3 radicals in spring (The solid lines indicate the mean concentration and the error bars indicate the standard error).

Figure S15. (a) Correlations between NO3_org_ratio_1 with PP of α-pinene, limonene, styrene and camphene during 2:00-6:00 for the spring campaign; (b) Correlation between LO-OOA with PP of α-pinene, limonene, styrene and camphene during 2:00-6:00 for the spring campaign; (c) Correlation between BC with PP of α -pinene, limonene, styrene and camphene during 2:00-6:00 for the spring campaign

Figure S16. Correlation of $NO_{3\_org\_ratio\_1}$ and NO_2 (a); $NO_{3\_org\_ratio\_1}$ and VOCs (the sum of α-pinene, limonene, styrene and camphene) (b); $NO_{3\_org\_PMF}$ and NO_2 (c) and $NO_{3\_org\_PMF}$ and VOCs (the sum of α-pinene, limonene, styrene and camphene) (d) during the springtime.

Table S1. The correlation coefficients (R) of $NO_{3,\ org}$ and $NO_{3,\ inorg}$ in 3- to 5-factors solutions estimated by PMF method with these estimated by NOx method, respectively.

Table S2. The mass fraction of NO+ and NO2+ in OA factors when FPEAK is 0 and the standard deviations (SD) of NO+ and NO2+ in OA factors across different FPEAK values (from –1.0 to 1.0).

Table S3. The average campaign concentrations of VOCs measured with an automated in situ gas-chromatography mass spectrometer (GC-MS), their reaction rate coefficients for reacting with NO_3 radicals and the production potential from NO3+VOC in spring.

Text S1: Nitrate radicals estimation

The approach of nitrates radical estimation is similar to Xu et al. (2015). Noted that only springtime NO_3 radicals are calculated because only VOCs concentrations have been measured in spring. The average concentration of VOCs and the reaction rate coefficients of NO_3 + VOCs at 25 ˚C at night are listed in Table S3. NO_3 radical is the product of NO_2+O_3, and its losses react with individual VOCs, NO and photolysis. Due to the existence of N_2O_5 in equilibrium with NO_2+ NO_3, we should first estimate the sinks of N_2O_5 impcting the life of nitrate radicals. There are both heterogenous and homogeneous reactions of N_2O_5 with water. The N_2O_5 lifetime, with respect to the heterogeneous uptake of aqueous particles, is (Dentener and Crutzen, 1993):

$$\tau_{N2O5,het} = \frac{1}{K_{het}} = \frac{4}{SA \cdot \gamma \cdot \nu} \quad (1)$$

where K_{het} represents the rate of heterogeneous uptake, SA represents the surface area of the particles calculated from the size-resolved particle number concentrations assuming spherical particles measured by SMPS, and then the SA under dry condition should be converted to ambient (wet) aerosol SA. In this study, the average ambient (wet) aerosol SA is 475 μm^2 cm^{-3} corrected by using the hygroscopic growth factor in Liu et al. (2010). γ is the uptake coefficient and we use the upper-limit values of 0.04 according on uptake coefficient on liquid water measurement (Saunders et al., 2003), ν represents the

molecular speed ($2.3*10^4$ cm s^{-1}), this gives an average N_2O_5 lifetime $\tau_{N2O5,het}$ of 915s. In addition, the N_2O_5 lifetime, with respect to the reaction with H_2O, is (Crowley et al., 2011):

$$\tau_{N2O5,H2O} = \frac{1}{K_{H2O}} = \frac{1}{2.5\times10^{-22}[H_2O]+1.8\times10^{-39}[H_2O]2} \quad (2)$$

K_{H2O} represents the reaction rate of N_2O_5 and H_2O, and $[H_2O]$ represents the water concentration (unit of molecule cm^{-3}); the daily maximum $[H_2O]$ is $5.5*10^{17}$ molecule cm^{-3} at 6:00 during the sampling period, and the calculated value is 1470 s. Then, we estimate the NO_3 lifetime by only considering the reaction with VOCs ($\tau_{NO3,VOCs}$):

$$\tau_{NO3,VOCs} = \frac{1}{\sum k_{i[VOC_i]}} \quad (3)$$

The average lifetime of NO_3 is approximately 14.08 s. Based on the estimation of the N_2O_5 and NO_3 lifetimes above, we can conclude that the influence of N_2O_5 could be ignored when estimating the NO_3 concentration and, due to the high reactivity of NO_3 (14.08 s), the steady-state NO_3 can be predicted:

$$[NO_3\cdot] = \frac{k_1[O_3][NO_2]}{J_{NO3}+k_2[NO]+\sum k_i[VOC_i]} \quad (4)$$

where J_{NO3} is calculated from the solar zenith angles and NO_3 photolysis rates (Saunders et al., 2003) and, in this study, the typical value of J_{NO3} is 0.12 s^{-1} during the daytime. k_1 is $3.52*10^{-17}$ cm^3 $molecule^{-1}$ s^{-1}, and k_2 is $2.7*10^{-11}$ cm^3 $molecule^{-1}$ s^{-1} according to the Master Chemical Mechanism model (http://mcm.leeds.ac.uk/MCM/; under 25 ˚C).

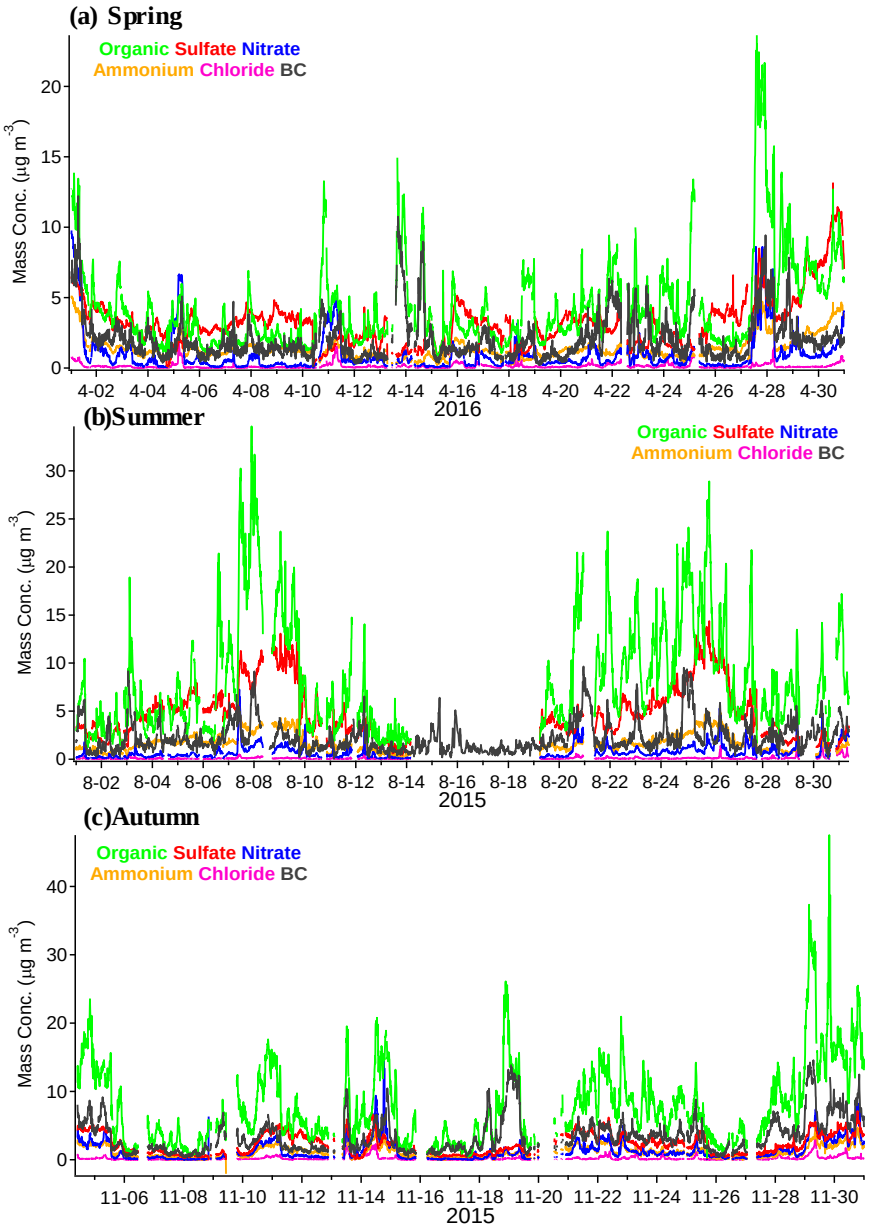

Figure S1. Time series of PM_1 species for spring (a), summer (b) and autumn (c).

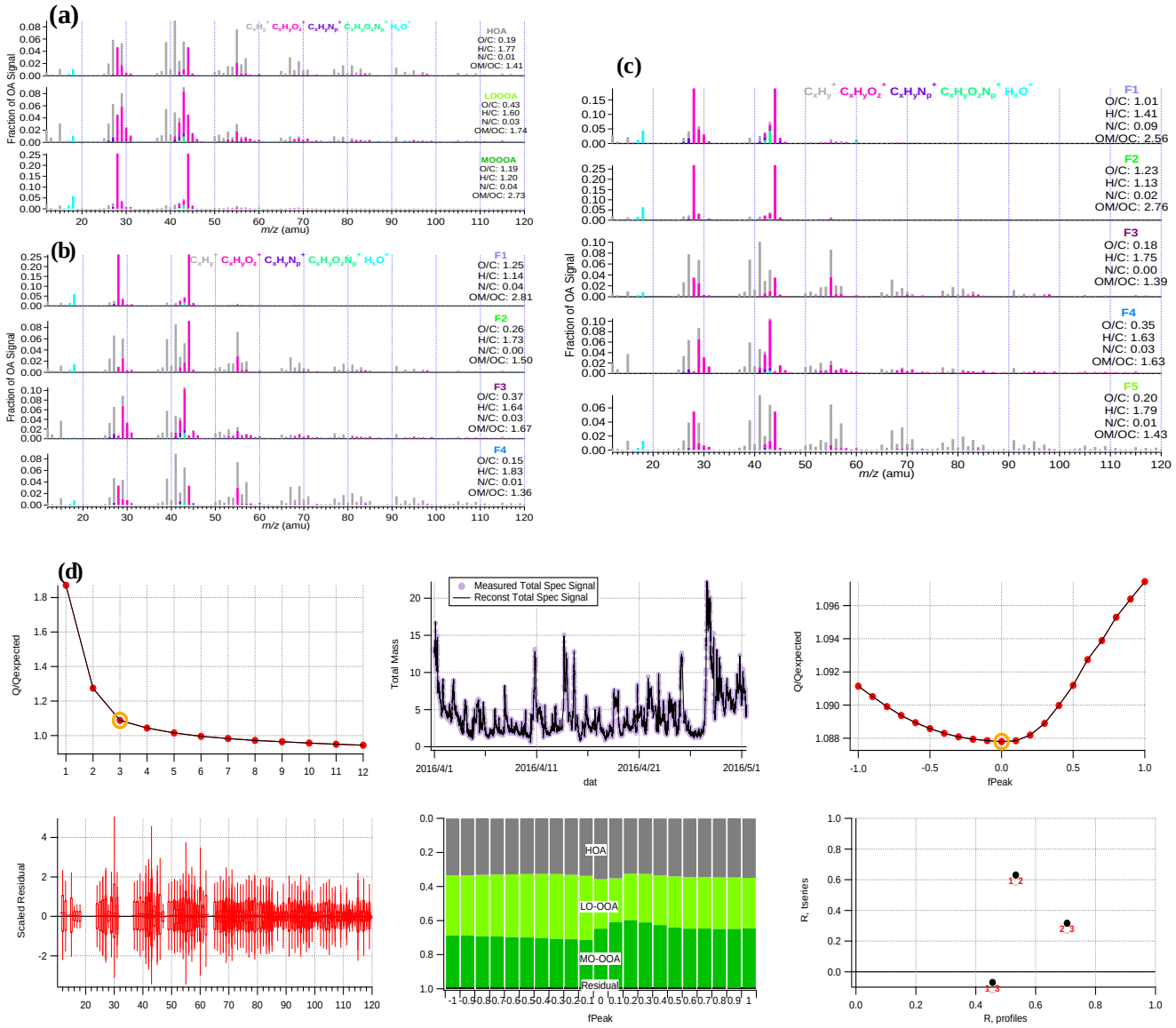

Figure S2. Mass spectrum profiles of 3 factors (a), 4 factors (b) and 5 factors (c) based on PMF analysis, and diagnostic plots of the chosen (3 factors) PMF solution (d) for spring: (1) Q/Qexp vs number of factors; (2) the time series of the measured and the reconstructed organic mass; (3) Q/Qexp vs. FPEAK for the solution with optimal number of factors; (4) the distribution of scaled residuals for each m/z; (5) mass fraction of PMF factors vs. FPEAK; (6) correlations of time series and mass spectra among PMF factors.

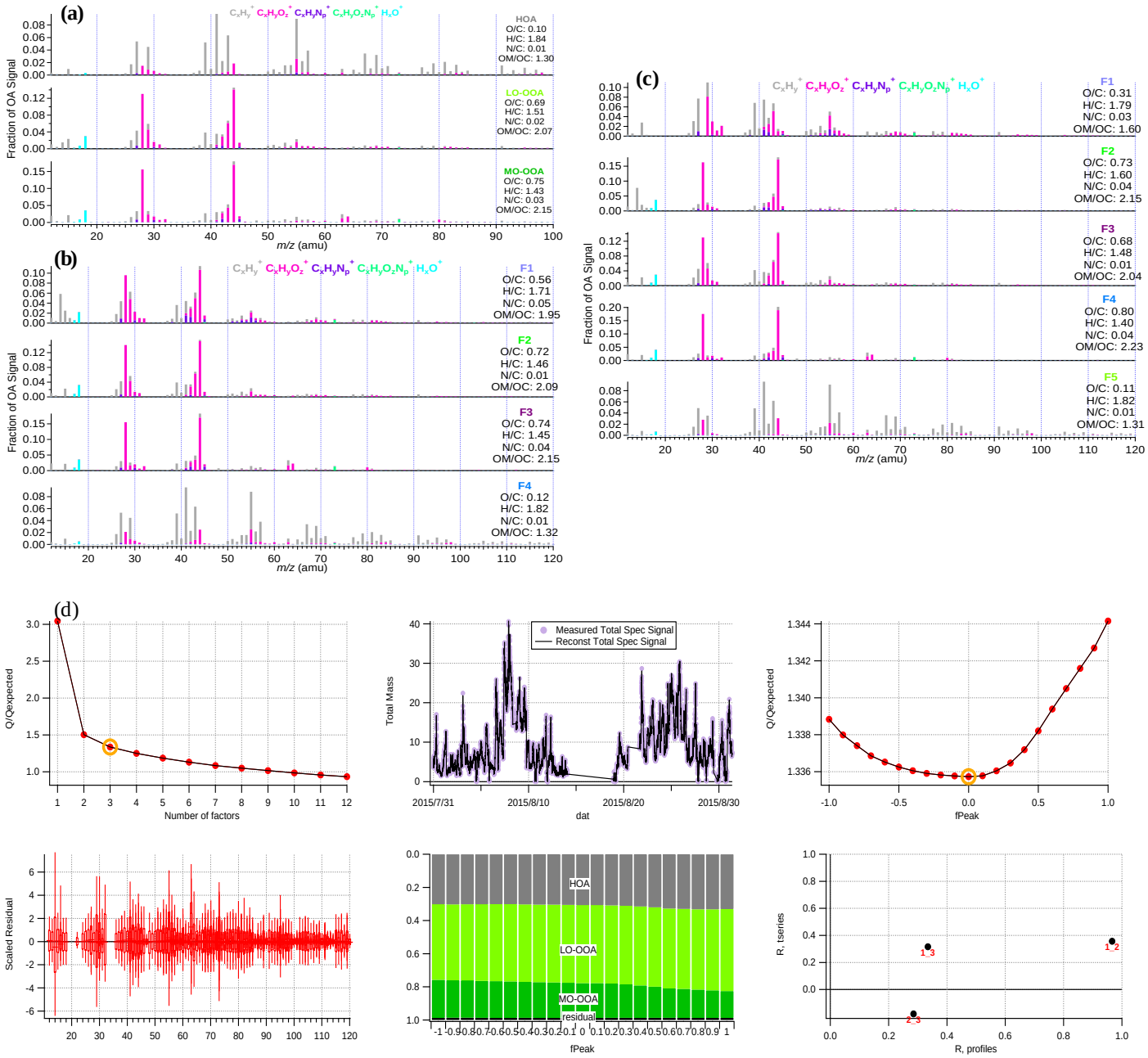

Figure S3. Mass spectrum profiles of 3 factors (a), 4 factors (b) and 5 factors (c) based on PMF analysis, and diagnostic plots of the chosen (3 factors) PMF solution (d) for summer: (1) Q/Qexp vs number of factors; (2) the time series of the measured and the reconstructed organic mass; (3) Q/Qexp vs. FPEAK for the solution with optimal number of factors; (4) the distribution of scaled residuals for each m/z; (5) mass fraction of PMF factors vs. FPEAK; (6) correlations of time series and mass spectra among PMF factors.

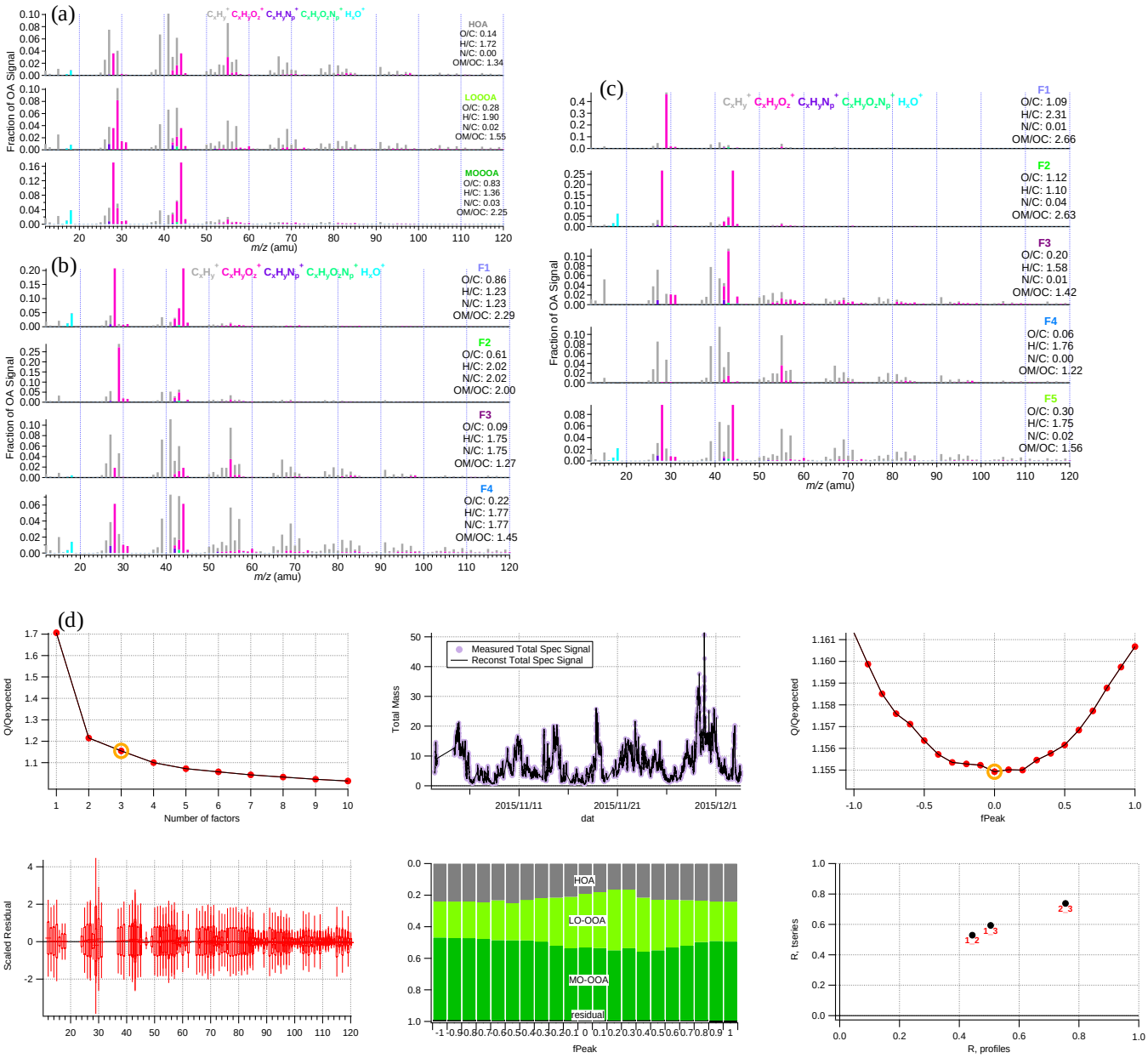

Figure S4. Mass spectrum profiles of 3 factors (a), 4 factors (b) and 5 factors (c) based on PMF analysis, and diagnostic plots of the chosen (3 factors) PMF solution (d) for Autumn: (1) Q/Qexp vs number of factors; (2) the time series of the measured and the reconstructed organic mass; (3) Q/Qexp vs. FPEAK for the solution with optimal number of factors; (4) the distribution of scaled residuals for each m/z; (5) mass fraction of PMF factors vs. FPEAK; (6) correlations of time series and mass spectra among PMF factors.

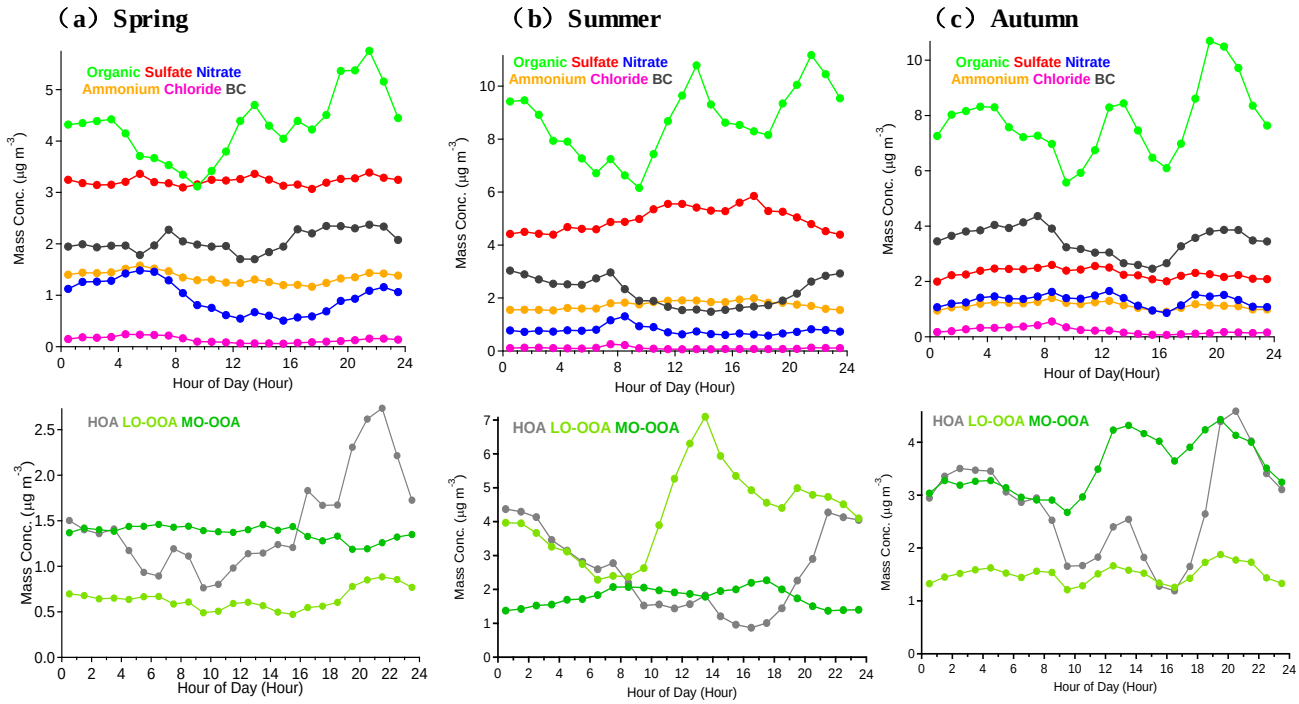

Figure S5. Diurnal cycles for NR-PM_1 species and OA factors in spring (a), summer (b) and autumn (c).

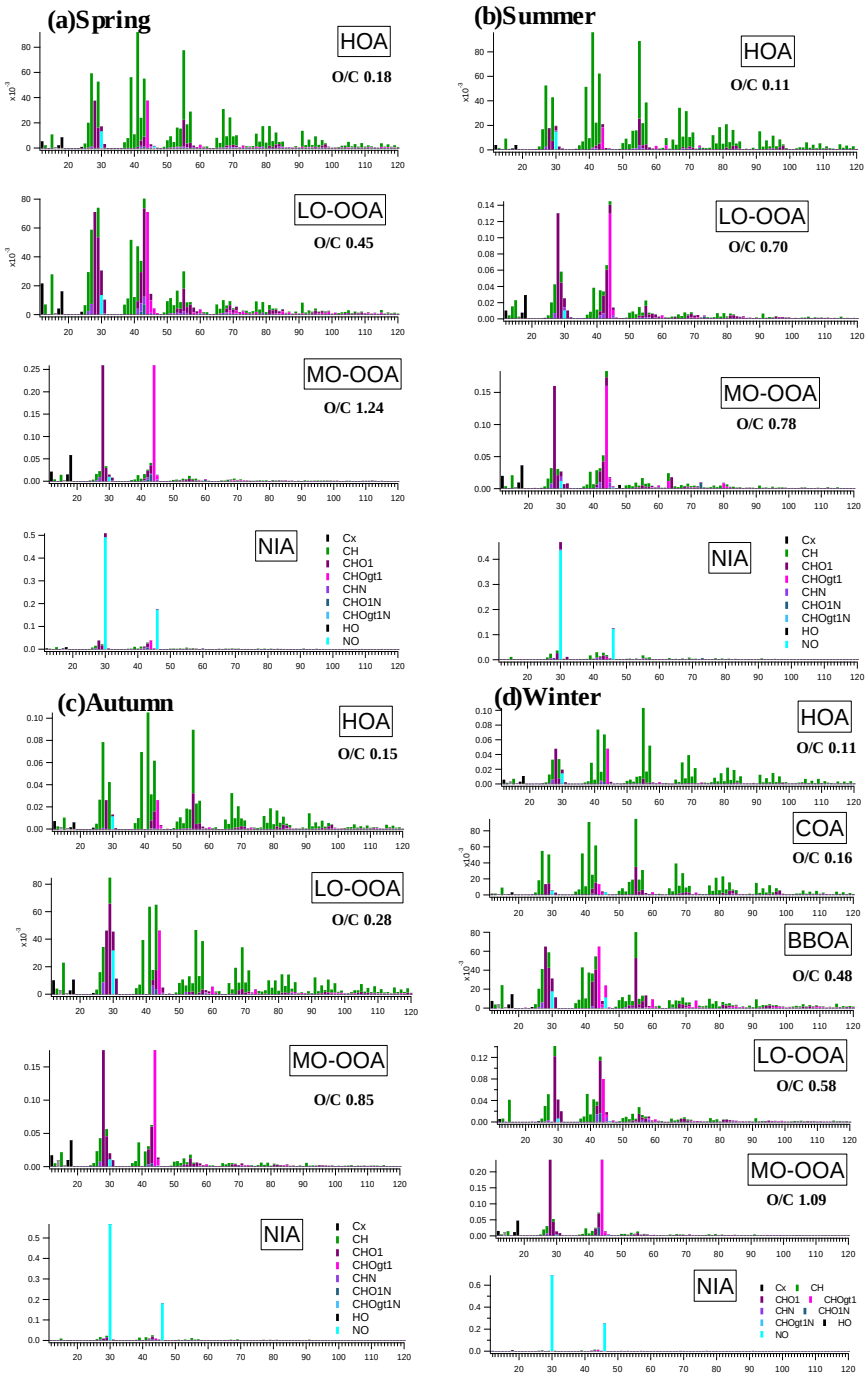

Figure S6. Mass spectra of OA factors resolved from the PMF analysis on high-resolution merged organic and nitrate mass spectra (i.e., $PMF_{org+NO3}$ analysis) for spring (a), summer (b), autumn(c) and winter (d).

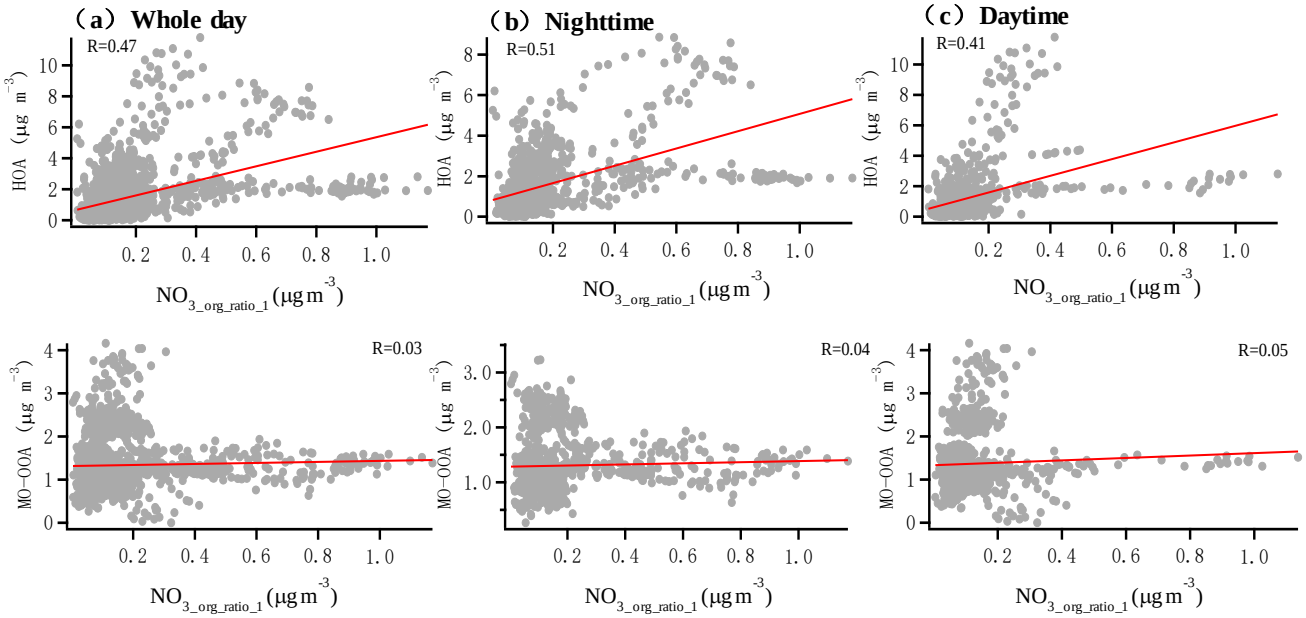

Figure S7. Scatter plots of $NO_{3\_org\_ratio\_1}$ with HOA and MO-OOA in spring for the whole day (a), at nighttime (b) and during the day (c).

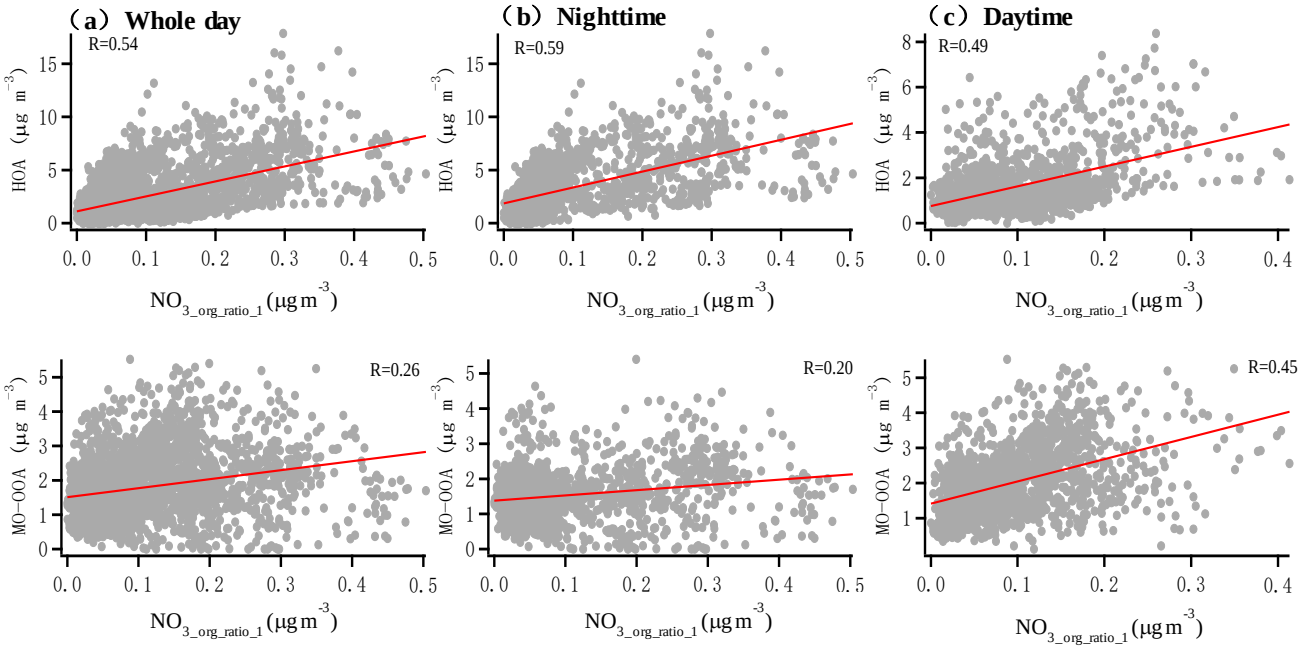

Figure S8. Scatter plots of $NO_{3\_org\_ratio\_1}$ with HOA and MO-OOA in summer for the whole day (a), at nighttime (b) and during the day (c).

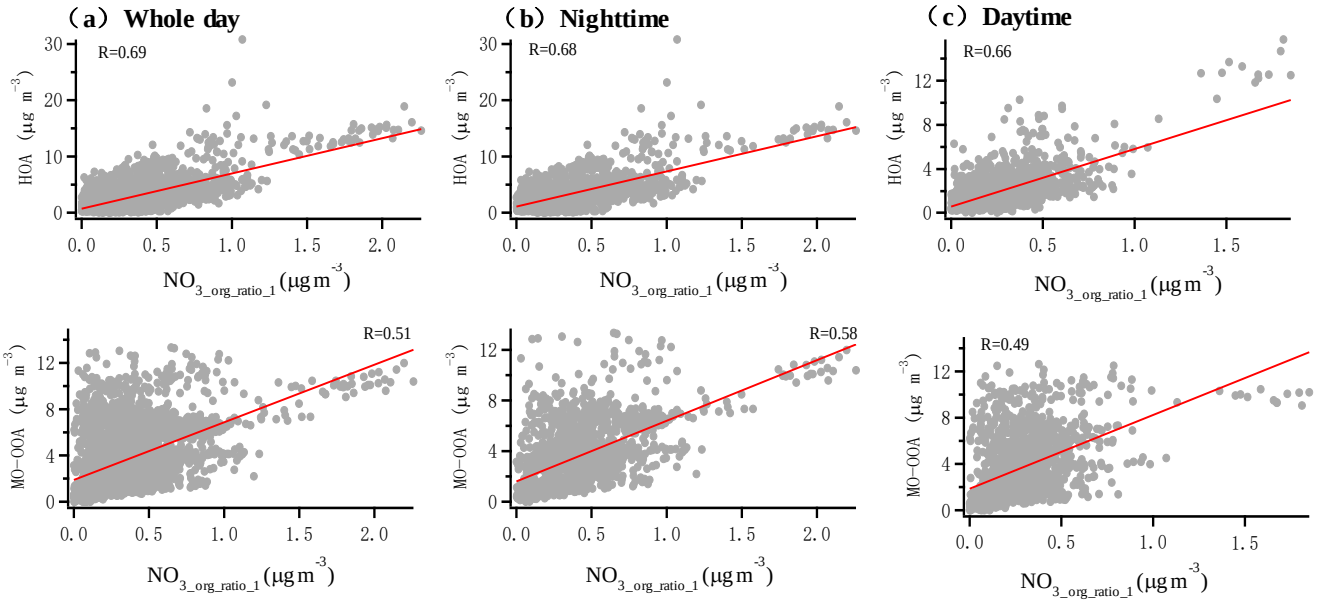

Figure S9. Scatter plots of $NO_{3\_org\_ratio\_1}$ with HOA and MO-OOA in autumn for the whole day (a), at nighttime (b) and during the day (c).

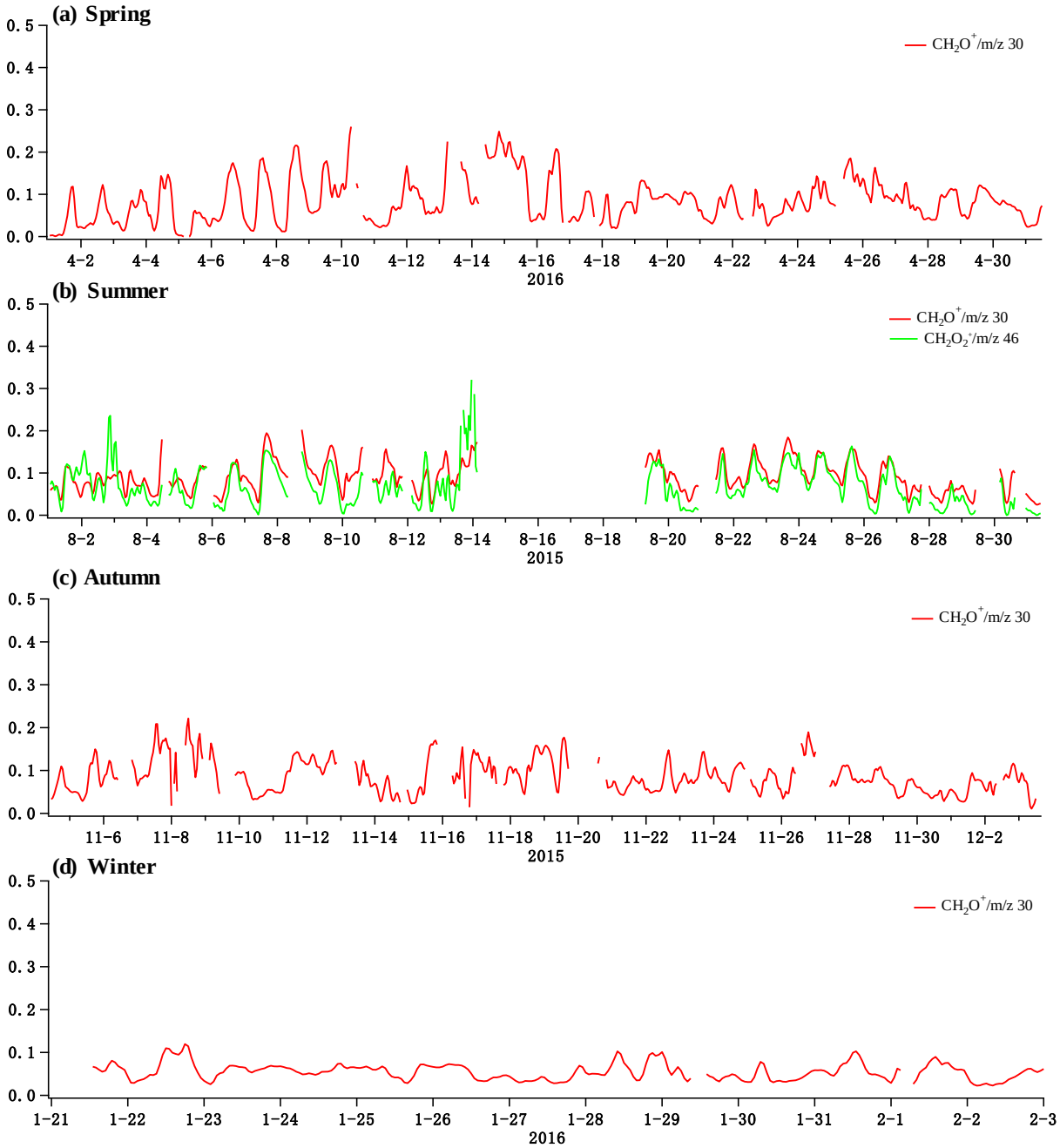

Figure S10. Time series of the contributions of CH_2O^+ in m/z 30 and $CH_2O_2^+$ in m/z 46 in the HR data of PM_1 for spring (a), summer (b), autumn (c) and winter (d). (High-resolution mass spectra at m/z 46 only contains NO_2^+ in spring, autumn and winter).

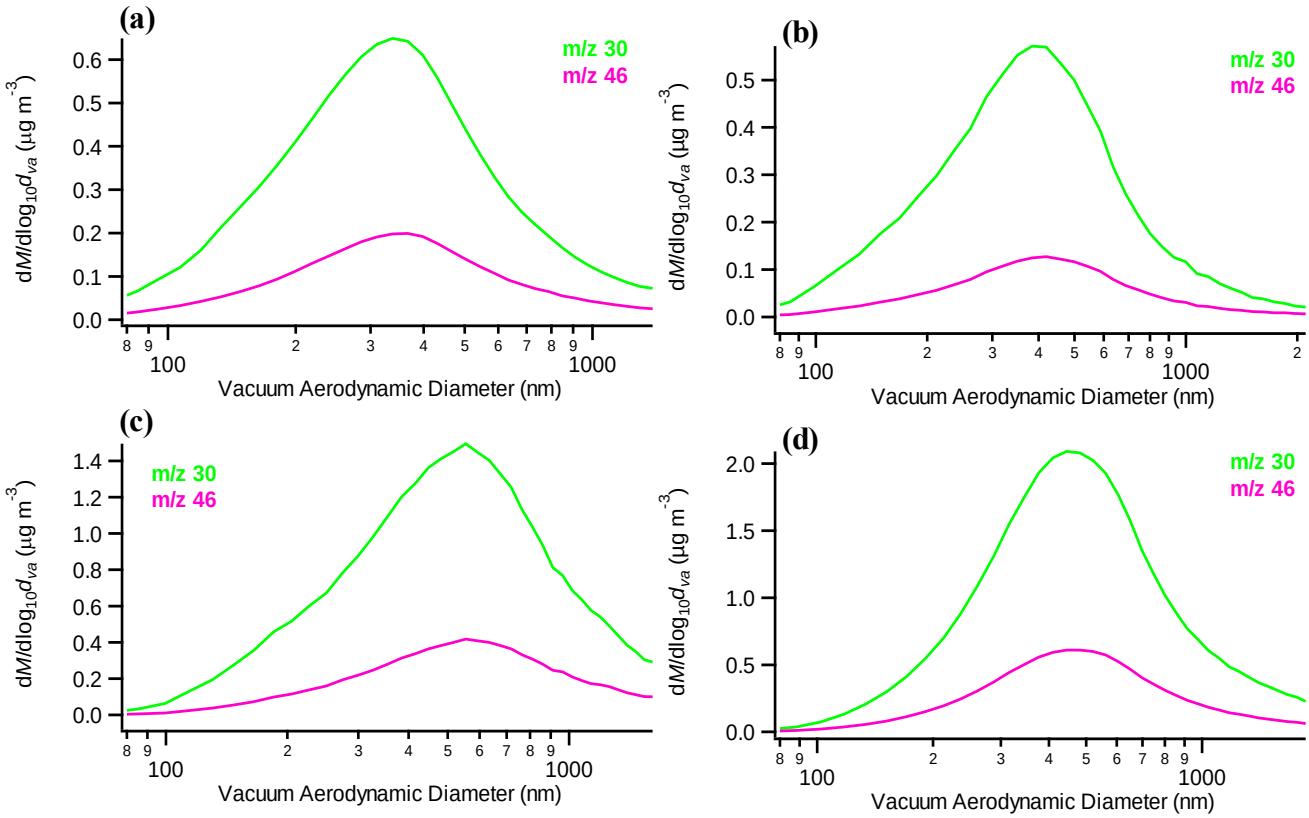

Figure S11. Average size distributions of m/z 30 and m/z 46 in spring (a), summer (b), autumn (c) and winter (d).

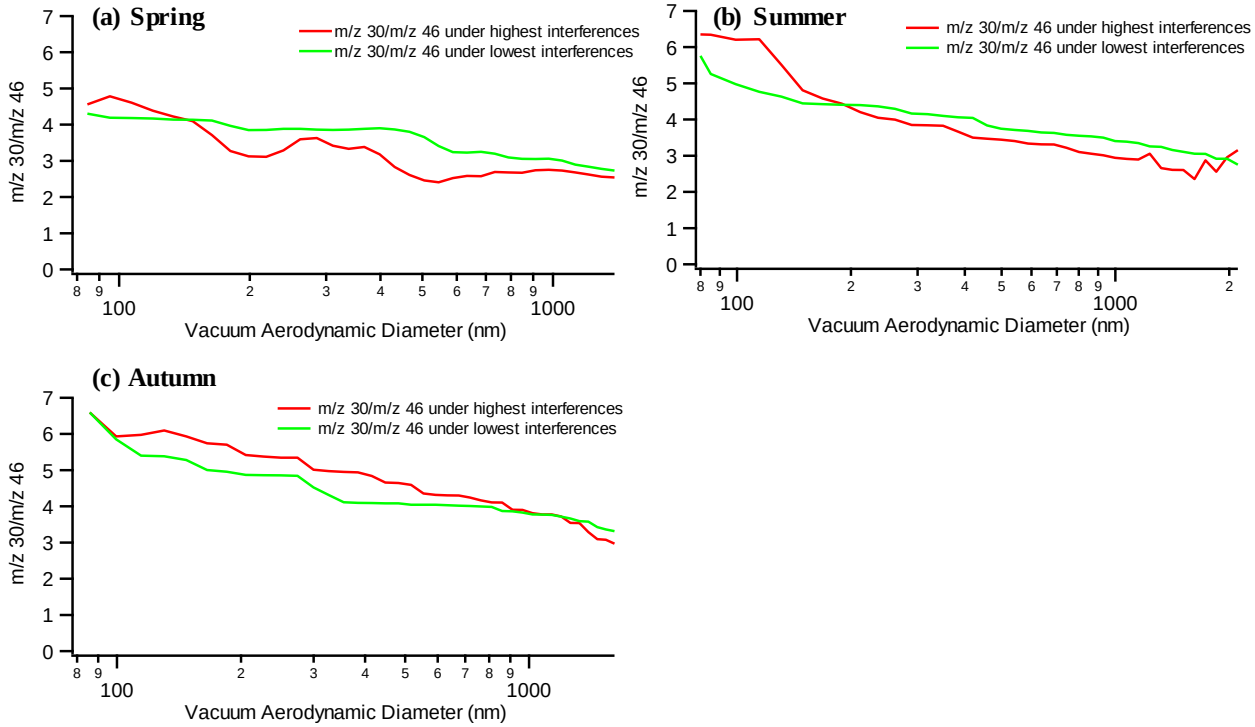

Figure S12. Average size distributions of m/z 30/m/z 46 ratio under under highest (>15%) and lowest interferences (<5%) $CH_2O_X^+$ interferences in spring (a), summer (b), autumn (c).

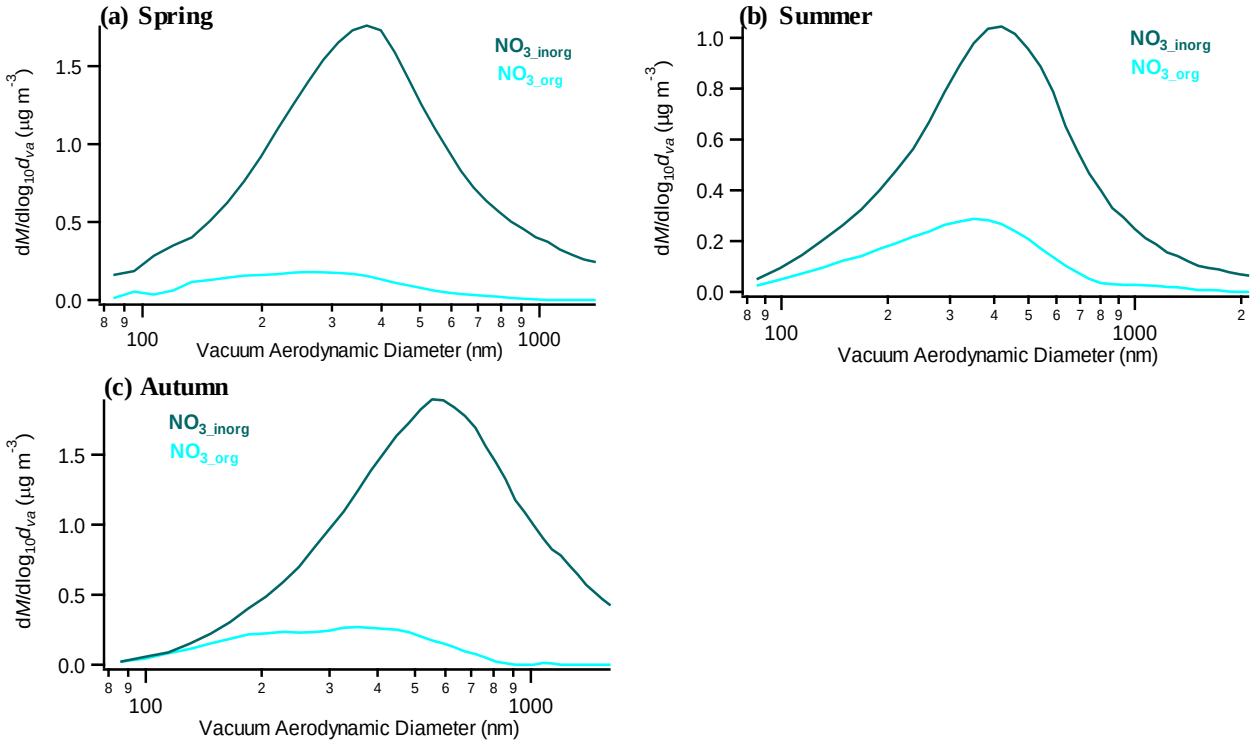

Figure S13. Average size distributions of organic and inorganic nitrates calculated using the size distributions of m/z 30/m/z 46 ratio and NO^+/NO_2^+ ratio method in spring (a), summer (b), autumn (c).

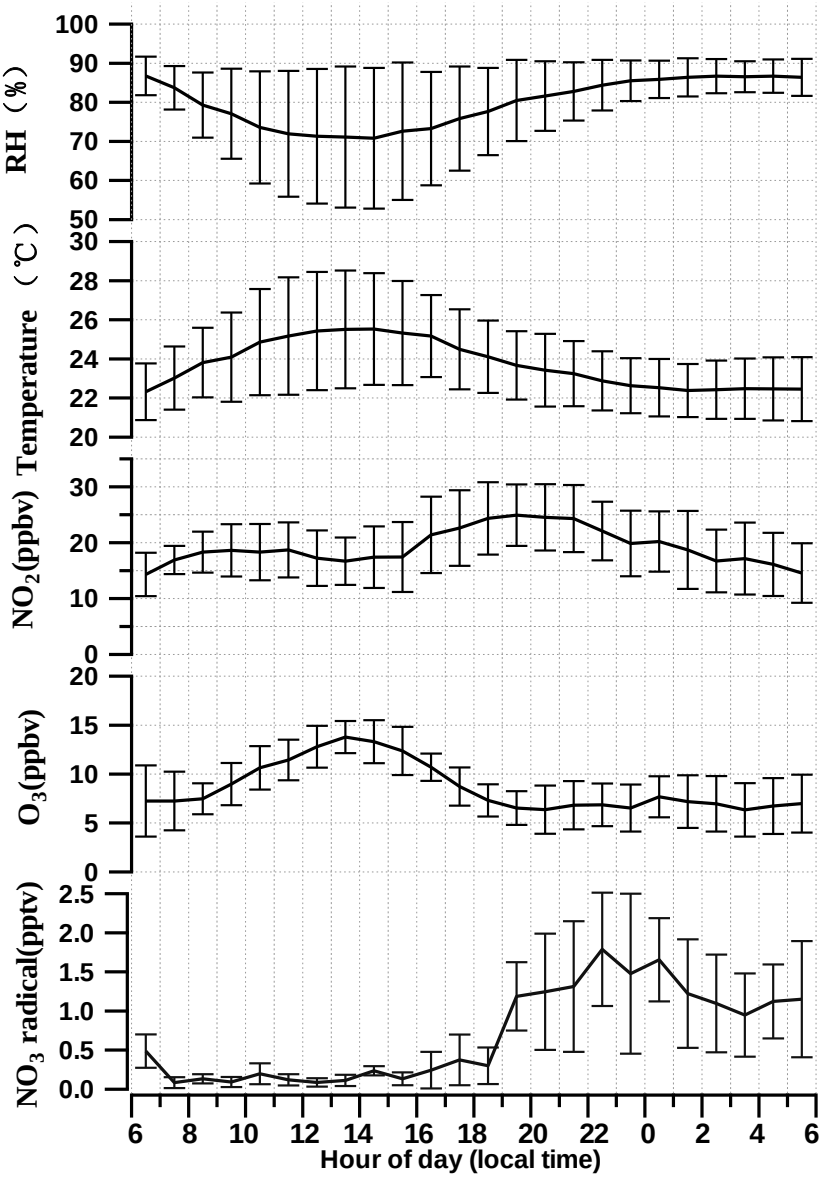

Figure S14. Diurnal trends of relative humidity (RH), temperature, NO_2, O_3 and calculated NO_3 radicals in spring (The solid lines indicate the mean concentration and the error bars indicate the standard error).

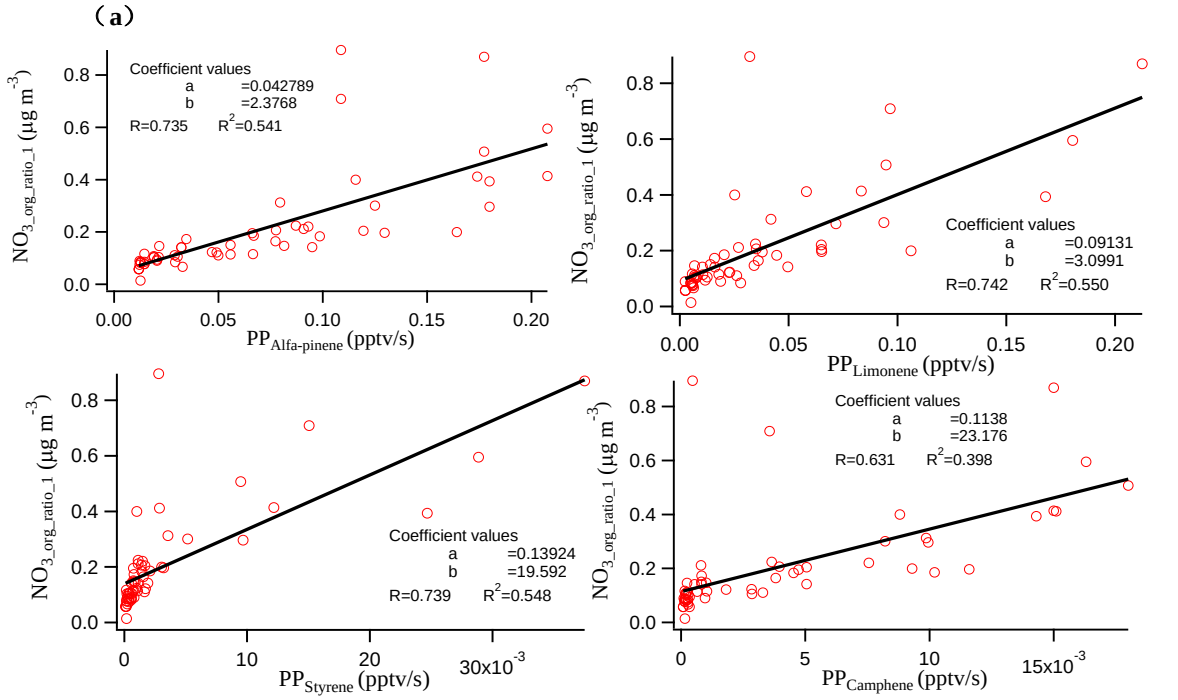
(a)
Coefficient values
a =0.042789
b =2.3768
R=0.735 R2=0.541
NO3_org_ratio_1 (μg m-3)
PPAlfa-pinene (pptv/s)
Coefficient values
a =0.09131
b =3.0991
R=0.742 R2=0.550
PPLimonene (pptv/s)
Coefficient values
a =0.13924
b =19.592
R=0.739 R2=0.548
PPStyrene (pptv/s)
30x10-3
Coefficient values
a =0.1138
b =23.176
R=0.631 R2=0.398
PPCamphene (pptv/s)
15x10-3

136

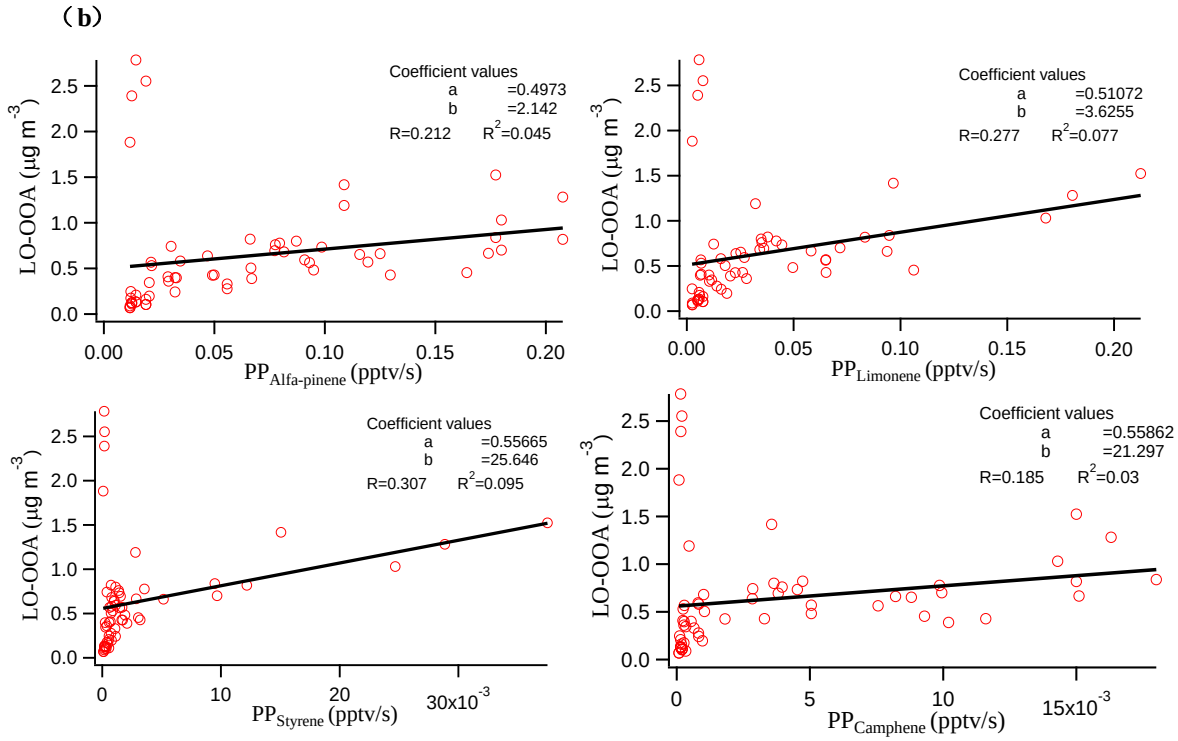
(b)
Coefficient values
a =0.4973
b =2.142
R=0.212 R2=0.045
LO-OOA (μg m-3)
PPAlfa-pinene (pptv/s)
Coefficient values
a =0.51072
b =3.6255
R=0.277 R2=0.077
PPLimonene (pptv/s)
Coefficient values
a =0.55665
b =25.646
R=0.307 R2=0.095
PPStyrene (pptv/s)
30x10-3
Coefficient values
a =0.55862
b =21.297
R=0.185 R2=0.03
PPCamphene (pptv/s)
15x10-3

137

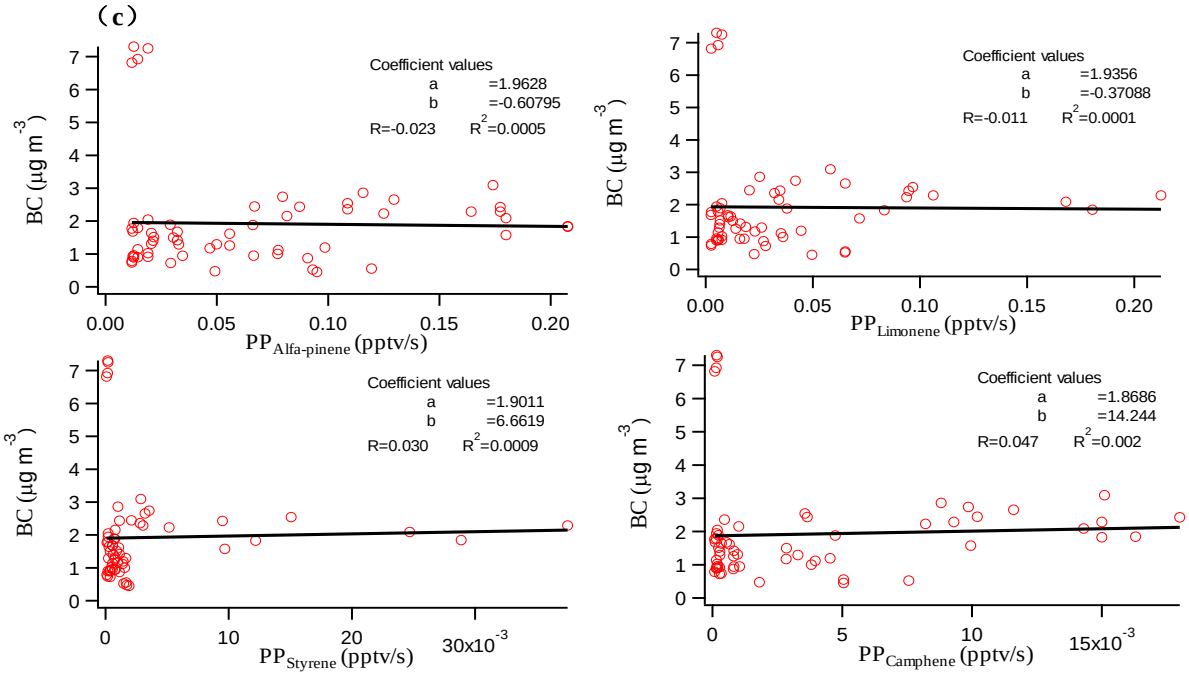

Figure S15. (a) Correlations between $NO_{3\_org\_ratio\_1}$ with PP of α-pinene, limonene, styrene and camphene during 2:00-6:00 for the spring campaign; (b) Correlation between LO-OOA with PP of α-pinene, limonene, styrene and camphene during 2:00-6:00 for the spring campaign; (c) Correlation between BC with PP of α-pinene, limonene, styrene and camphene during 2:00-6:00 for the spring campaign

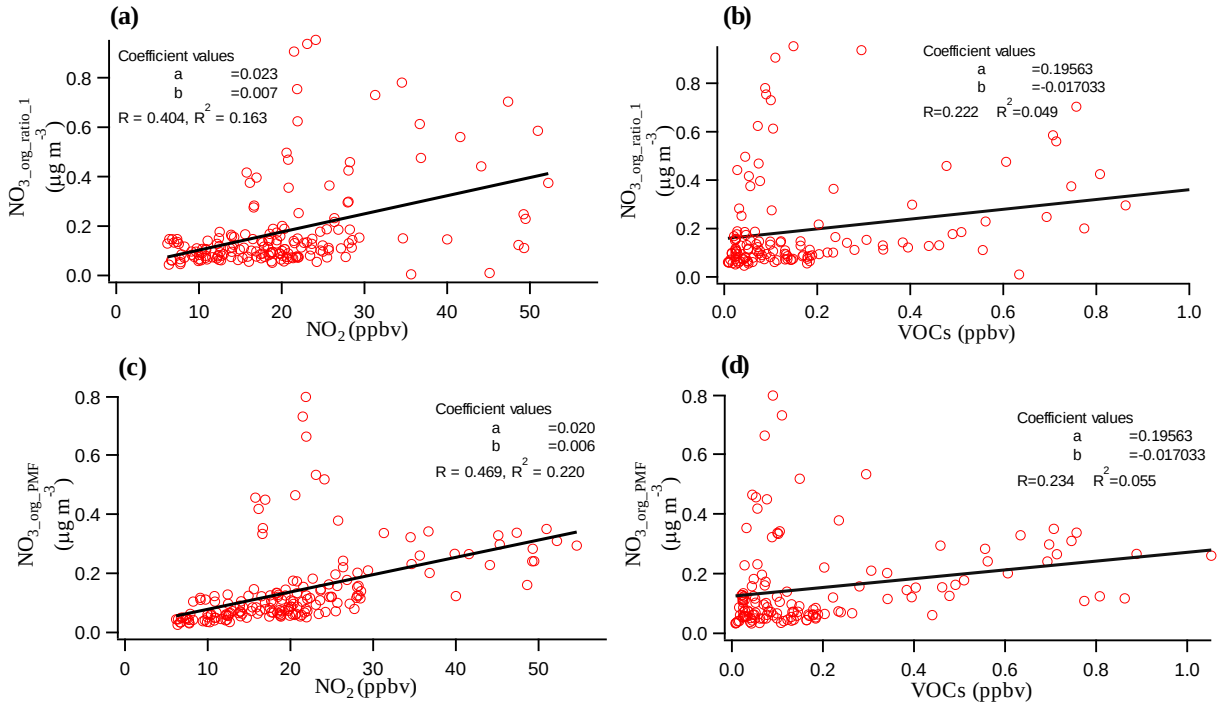

Figure S16. Correlation of $NO_{3\_org\_ratio\_1}$ and NO_2 (a); $NO_{3\_org\_ratio\_1}$ and VOCs (the sum of α-pinene, limonene, styrene and camphene) (b); $NO_{3\_org\_PMF}$ and NO_2 (c) and $NO_{3\_org\_PMF}$ and VOCs (the sum of α-pinene, limonene, styrene and camphene) (d) during the springtime.

Table S1. The correlation coefficients (R) of $NO_{3,\,org}$ and $NO_{3,\,inorg}$ in 3- to 5-factors solutions estimated by PMF method with these estimated by NOx method, respectively.

		3-factor solution		**4-factor solution**		**5-factor solution**	
		$NO_{3,org}$ (NOx vs. PMF)	$NO_{3,inorg}$ (NOx vs. PMF)	$NO_{3,org}$ (NOx vs. PMF)	$NO_{3,inorg}$ (NOx vs. PMF)	$NO_{3,org}$ (NOx vs. PMF)	$NO_{3,inorg}$ (NOx vs. PMF)
Spring	R	0.82	0.92	0.81	0.90	0.80	0.91
	Slope	1.21	0.76	1.15	0.78	1.20	0.82
Summer	R	0.82	0.87	0.82	0.88	0.81	0.90
	Slope	1.53	0.70	1.50	0.65	1.45	0.64
Autumn	R	0.77	0.86	0.75	0.85	0.76	0.83
	Slope	0.81	0.85	0.76	0.82	0.75	0.78

Table S2. The mass fraction of NO^+ and NO_2^+ in OA factors when FPEAK is 0 and the standard deviations (SD) of NO^+ and NO_2^+ in OA factors across different FPEAK values (from –1.0 to 1.0)

			HOA	LO-OOA	MO-OOA
Spring	NO^+	FPEAK =0	$1.3*10^{-2}$	$1.4*10^{-2}$	$9.8*10^{-3}$
		SD	$1.2*10^{-3}$	$6.9*10^{-4}$	$2.4*10^{-3}$
	NO_2^+	FPEAK =0	$1.2*10^{-2}$	$1.5*10^{-4}$	$3.0*10^{-8}$
		SD	$4.6*10^{-4}$	$2.0*10^{-5}$	$8.6*10^{-8}$
Summer	NO^+	FPEAK =0	$1.5*10^{-2}$	$1.0*10^{-2}$	$1.2*10^{-2}$
		SD	$6.8*10^{-4}$	$1.1*10^{-3}$	$2.0*10^{-3}$
	NO_2^+	FPEAK =0	$1.5*10^{-6}$	$6.7*10^{-4}$	$1.8*10^{-3}$
		SD	$2.4*10^{-7}$	$9.3*10^{-5}$	$3.5*10^{-4}$
Autumn	NO^+	FPEAK =0	$1.1*10^{-2}$	$3.1*10^{-2}$	$1.0*10^{-2}$
		SD	$2.2*10^{-3}$	$2.5*10^{-3}$	$2.7*10^{-3}$
	NO_2^+	FPEAK =0	$7.0*10^{-8}$	$9.8*10^{-8}$	$2.8*10^{-7}$
		SD	$2.5*10^{-9}$	$2.7*10^{-8}$	$3.0*10^{-8}$

Table S3. The average campaign concentrations of VOCs measured with an automated in situ gas-chromatography mass spectrometer (GC-MS), their reaction rate coefficients for reacting with NO_3 radical and the production potential from NO3+VOC in spring.

VOC species	Mean concentration (ppbv)	Rate Coefficient	Production potential (pptv/s)
1,2,3-Trimethylbenzene	0.057	1.90E-15	3.72E-06
1,2,4-Trimethylbenzene	0.177	1.80E-15	1.10E-05
1,3,5-Trimethylbenzene	0.051	8.80E-16	1.54E-06
1,3-Butadiene	0.052	1.00E-13	1.79E-04
1-Butene	0.415	1.32E-14	1.89E-04
1-Hexene	0.022	1.20E-14	9.06E-06
1-Pentene	0.022	1.20E-14	9.27E-06
2,2,4-Trimethylpentane	0.068	9.00E-17	2.10E-07
2,2-Dimethylbutane	0.199	4.40E-16	3.01E-06
2,3,4-Trimethylpentane	0.022	1.90E-16	1.44E-07
2,3-Dimethylbutane	0.299	4.40E-16	4.54E-06

2,3-Dimethylpentane	0.293	1.50E-16	1.51E-06
2-Methylheptane	0.034	1.90E-16	2.20E-07
2-Methylhexane	0.514	1.50E-16	2.66E-06
2-Methylpentane	1.582	1.80E-16	9.81E-06
3-Methylheptane	0.027	1.90E-16	1.74E-07
3-Methylhexane	0.534	1.50E-16	2.76E-06
3-Methylpentane	1.411	2.20E-16	1.07E-05
Acetaldehyde	1.249	2.70E-15	1.16E-04
Acetylene	0.941	5.10E-17	1.65E-06
Acrolein	0.042	3.30E-15	4.73E-06
Benzene	0.599	3.00E-17	6.19E-07
cis-2-Pentene	0.005	3.70E-13	6.57E-05
Cyclohexane	1.164	1.40E-16	5.61E-06
Cyclopentane	0.416	1.40E-16	2.00E-06
Ethane	1.567	1.00E-17	5.40E-07
Ethylbenzene	0.563	1.20E-16	2.34E-06
Isoprene	0.032	6.96E-13	7.76E-04
m/p-Xylene	0.602	3.80E-16	7.88E-06
Methacrolein	0.012	3.40E-15	1.44E-06
Methylcyclohexane	0.172	1.40E-16	8.29E-07
Methylcyclopentane	0.673	1.40E-16	3.25E-06
n-Butanal	0.044	1.10E-14	1.68E-05
n-Butane	1.848	4.60E-17	2.93E-06
n-Decane	0.060	2.80E-16	5.74E-07
n-Heptane	0.351	1.50E-16	1.81E-06
n-Hexane	1.916	1.10E-16	7.25E-06
n-Nonane	0.033	2.30E-16	2.59E-07
n-Pentanal	0.128	1.50E-14	6.61E-05
n-Pentane	0.593	8.70E-17	1.78E-06
n-Propylbenzene	0.029	6.00E-16	6.01E-07
Octane	0.064	1.90E-16	4.17E-07
o-Xylene	0.464	3.80E-16	6.06E-06

Propanal	0.144	6.31E-15	3.12E-05
Propane	3.678	7.00E-17	8.86E-06
Propene	0.477	9.54E-15	1.57E-04
Styrene	0.194	1.50E-12	1.00E-02
Toluene	3.120	7.00E-17	7.52E-06
Alpha-Pinene	0.391	6.21E-12	8.36E-02
Beta-Pinene	0.013	2.51E-12	1.10E-03
Camphene	0.276	6.20E-13	5.91E-03
Limonene	0.137	1.22E-11	5.77E-02

References

Crowley, J.N., Thieser, J., Tang, M.J., Schuster, G., Bozem, H., Beygi, Z.H., Fischer, H., Diesch, J.M., Drewnick, F., Borrmann, S., Song, W., Yassaa, N., Williams, J., Pöhler, D., Platt, U., Lelieveld, J.: Variable lifetimes and loss mechanisms for NO3and N2O5during the DOMINO campaign: Contrasts between marine, urban and continental air. Atmos. Chem. Phys. 11, 10853-10870, https://doi.org/10.5194/acp-11-10853-2011, 2011.

Dentener, F. J. and Crutzen, P. J.: Reaction of N2O5 on tropospheric aerosols: Impact on the global distributions of NOx , O3, and OH, J. Geophys. Res., 98, 7149–7163, https://doi.org/10.1029/92JD02979, 1993.

Liu, X.G., Zhang, Y.H., Wen, M.T., Wang, J.L., Jung, J.S., Chang, S.-Y., Hu, M., Zeng, L.M. and Kim, Y.J.: A closure study of aerosol hygroscopic growth factor during the 2006 Pearl River Delta Campaign. Adv. Atmos. Sci, 27, 947–956, https://doi.10.1007/s00376-009-9150-z, 2010.

Saunders, S.M., Jenkin, M.E., Derwent, R.G., Pilling, M.J.: Protocol for the development of the Master Chemical Mechanism, MCM v3 (Part A): tropospheric degradation of non-aromatic volatile organic compounds. Atmos. Chem. Phys. 3, 161–180, https://doi.org/10.5194/acp-3-161-2003, 2003.

Xu, L., Guo, H., Boyd, C.M., Klein, M., Bougiatioti, A., Cerully, K.M., Hite, J.R., Isaacman-VanWertz, G., Kreisberg, N.M., Knote, C., Olson, K., Koss, A., Goldstein, A.H., Hering, S. V., de Gouw, J., Baumann, K., Lee, S.-H., Nenes, A., Weber, R.J., Ng, N.L.: Effects of anthropogenic emissions on aerosol formation from isoprene and monoterpenes in the southeastern United States. Proc. Natl. Acad. Sci. 112, 37-42, https://doi.org/10.1073/pnas.1417609112, 2015.